Life Sciences in Space Research 39 (2023) 119–130

Contents lists available at ScienceDirect

Life Sciences in Space Research

journal homepage: www.elsevier.com/locate/lssr

Comparison of the particle flux measured by Liulin-MO dosimeter in ExoMars TGO science orbit with those calculated by models

Jordanka Semkova [a,*], Victor Benghin [b], Jingnan Guo [c,d], Jian Zhang [c], Fabiana Da Pieve [e], Krasimir Krastev [a], Yuri Matviichuk [a], Borislav Tomov [a], Vyacheslav Shurshakov [b], Sergey Drobyshev [b], Igor Mitrofanov [f], Dmitry Golovin [f], Maxim Litvak [f]

[a] Space Research and Technology Institute, Bulgarian Academy of Sciences, Sofia, Bulgaria
[b] Institute of Biomedical Problems of the Russian Academy of Sciences, Moscow, Russia
[c] Deep space Exploration Laboratory, University of Science and Technology of China, Hefei, China
[d] CAS Center for Excellence in Comparative Planetology USTC, Hefei, China
[e] Royal Belgian Institute for Space Aeronomy, BIRA-IASB, Brussels, Belgium
[f] Space Research Institute, Russian Academy of Sciences, Moscow, Russia

ARTICLE INFO

Keywords:
Mars orbit
Galactic cosmic rays
Albedo radiation
Radiation flux calculation
Radiation flux measurement

ABSTRACT

The knowledge of the space radiation environment in spacecraft transition and in Mars vicinity is of importance for the preparation of the human exploration of Mars. ExoMars Trace Gas Orbiter (TGO) was launched on March 14, 2016 and was inserted into circular Mars science orbit (MSO) with a 400 km altitude in March 2018. The Liulin-MO dosimeter is a module of the Fine Resolution Epithermal Neutron Detector (FREND) aboard ExoMars TGO and has been measuring the radiation environment during the TGO interplanetary travel to Mars and continues to do so in the TGO MSO. One of the scientific objectives of the Liulin-MO investigations is to provide data for verification and benchmarking of the Mars radiation environment models. In this work we present results of comparisons of the flux measured by the Liulin-MO in TGO Mars orbit with calculated estimations. Described is the methodology for estimation the particle flux in Liulin-MO detectors in MSO, which includes modeling the albedo spectra and procedure for calculation the fluxes, recorded by Liulin-MO on the basis of the detectors shielding model. The galactic cosmic rays (GCR) and Mars albedo radiation contribution to the detectors count rate was taken into account. The GCR particle flux was calculated using the Badhwar O'Neil 2014 model for December 1, 2018. Detailed calculations of the albedo spectra of protons, helium ions, neutrons and gamma rays at 70 km height, performed with Atmospheric Radiation Interaction Simulator (AtRIS), were used for deriving the albedo radiation fluxes at the TGO altitude. In particular, the sensitivity of the Liulin-MO semiconductor detectors to neutron and gamma radiation has been considered in order to calculate the contribution of the neutral particles to the detected flux. The results from the calculations suggest that the contribution of albedo radiation can be about 5% of the measured total flux from GCR and albedo at the TGO altitude. The critical effect of TGO orientation, causing different shading of the GCR flux by Mars, is also analysed in detail. The comparison between the measurements and estimations shows that the measured fluxes exceed the calculated values by at least 20% and that the effect of TGO orientation change is approximately the same for the calculated and measured fluxes. Accounting for the ACR contribution, secondary radiation and the gradient of GCR spectrum from 1 AU to 1.5 AU, the calculated flux may increase to match the measurement results. The results can serve for the benchmarking of GCRs models at Martian orbit.

1. Introduction

The radiation environment on Mars and its vicinity can be very hazardous for future human exploration of the red planet. Because of its thin atmosphere and the lack of global intrinsic magnetic field, Mars is very exposed to space radiation. The primary space radiation reaching Mars is constituted mostly by galactic cosmic rays (GCR) and sporadically by Solar Energetic Particles (SEP) resulted from transient solar

* Corresponding author.
E-mail address: jsemkova@stil.bas.bg (J. Semkova).

https://doi.org/10.1016/j.lssr.2022.08.007
Received 25 May 2022; Received in revised form 14 August 2022; Accepted 20 August 2022
Available online 24 August 2022

events such as flares and coronal mass ejections. Both these primary radiation populations create downward secondaries in the thin Martian atmosphere, by inelastic interactions with the atmospheric atomic nuclei. Ionization and nuclear-inelastic scattering processes such as fragmentation and spallation create cascades of downward secondaries. The radiation (either primary or secondary) that has not lost all its energy in interactions with the atmosphere reaches the ground, and creates further secondary upward radiation when interacting with the Martian regolith (Saganti et al., 2004; Kim et al., al.,2014). As a consequence, the radiation field on Mars is complex, composed by both charged and neutral particles that can be downward - or upward - directed.

Understanding the health-induced risks that human explorers will encounter both during the interplanetary travel and on the Martian surface is key for planning future crewed missions to the red planet (https://humanresearchroadmap.nasa.gov/evidence/reports/Cancer.pdf). There exist by now a number of studies done in the last two decades on the radiation environment induced by GCR at Mars (Saganti et al., 2004; De Angelis et al., 2006; Schwadron et al., 2010; Ehresmann et al., 2011; McKenna-Lawlor et al., 2012; Gronoff et al., 2015; Guo et al., 2015; Matthiä et al., 2016; Matthiä and Berger, 2017; Röstel et al., 2020; Gonçalves et al., 2022; Guo et al., 2021).

The detection of neutral particles, such gamma rays and neutrons, is particularly challenging. Neutrons are generated with energies of few hundreds of MeV and lower by the interaction of charged particles with the atmosphere and by the interaction of the radiation reaching the ground with the regolith, via evaporation of excited nuclei. Neutrons do not undergo electromagnetic interactions and can thus penetrate matter easily. The Martian gamma and neutron fluxes and spectra were derived from Mars Science Laboratory (MSL) Radiation Assessment Detector (RAD) neutral particle measurements during the early phase of the mission in (Guo et al., 2017), using an inversion method, and were compared to the results from different particle transport models such as GEANT4, HZETRN, MCNP6 and PHITS (Matthiä et al., 2017). The comparison showed that for gamma-rays, almost all modeled photon spectra agree well within a factor of about two with the RAD data. However, for neutron spectra, the comparison of the models amongst each other and with the RAD data revealed some discrepancies up to about one order of magnitude. The discrepancies may result from both the detection method and statistical constraints and the uncertainties in the model used to simulate the radiation response functions, as well as the uncertainties in different nuclear models. So the overall understanding of the radiation environment associated to neutral particles at Mars is not yet fully satisfying.

The radiation environment at Martian orbit has been less studied, with a recent boost by the measurements on the TGO ExoMars spacecraft (Semkova et al., 2018, 2021). Previous measurements on the GCR flux and spectra are from Mars Odyssey, whose radiation detector, the Martian Radiation Environment Experiment (MARIE), stopped working during the SEP events of October 2003, but data could still be retrieved from the Gamma Ray Spectrometer and the scintillator component of the High Energy Neutron Detector (Zeitlin et al., 2010). Recent studies have also analyzed data from Mars Express (Knutsen et al., 2021). The ExoMars TGO spacecraft carries the Fine Resolution Epithermal Neutron Detector (FREND), one module of the latter being the Liulin-MO dosimeter (Mitrofanov et al., 2018), a charged (and neutral) particle detector that has been providing in-situ measurements that constitute an important data set for understanding the radiation environment, during the TGO interplanetary travel and in Martian orbit.

Liulin-MO data about the radiation environment during the TGO cruise to Mars and in high elliptic Mars orbits (Mars capture orbits MCO1 with 98,000 - 230 km altitude and MCO2 with 37,150 - 200 km altitude) covers the period from April 2016 to March 2017 (Semkova et al., 2018). Since May 2018 Liulin-MO investigates the radiation conditions in Mars science orbit (MSO) which is a circular orbit with 400 km altitude, 74° inclination, ~ 2 h orbit period.

One of the scientific objectives of the Liulin-MO investigations is to provide data for verification and benchmarking of the radiation environment models and assessment of the radiation risk to the crewmembers of future exploratory flights (Semkova et al., 2018).

Models of GCR describe their spectra and intensity in free space, away from any celestial body. Comparison of several GCR models results and Liulin-MO measurements of the dose rate and particle fluxes of GCR in the interplanetary space were discussed in Benghin et al. (2019). The comparison of Matthiä et al. (2013) GCR model results with Liulin-MO measurements during the transit to Mars and on the high elliptic orbit shows that the measured dose rate behind the shielding of the detectors of Liulin-MO is about 25% higher than the simulated values (Semkova et al., 2021).

To use Liulin-MO data measured at Mars circular orbit for benchmarking of the radiation environment models, the shading of GCR by Mars and the contribution of albedo particles from Mars atmosphere and surface to the measured flux should be taken into account.

Preliminary attempts to estimate the effect of Mars presence on the measured fluxes and dose rates in TGO MSO have been done. In Mars circular orbit the planet shades single detectors' field of view (FOV), thus reducing part of free-space GCR flux. The shaded part of FOV is an angle dependent on TGO orientation and altitude. TGO orientation can vary by 180° though not often; TGO altitude varies within 50 (±25) km in every orbital pass. The dependence of the flux and dose rate measured by Liulin-MO on the distance of TGO from Mars and the orientation of dosimeter detectors was investigated (Krastev et al., 2019). To account for the albedo particles contribution to the measured flux we used the measurements conducted near the pericenter in high elliptic TGO orbits MCO1 and MCO2 and compared them with the measurements in the apocenter where the influence of Mars presence on the measured values is negligible (Semkova et al., 2020). We have analysed all 38 cases of data available for pericenter crossing during Mars capture orbit phase of TGO. A statistical study from these cases gives albedo contribution of 6 – 12 percent to the measured flux. These previous investigations clearly demonstrated that to estimate the albedo contribution correctly one need to know at 400 km height above Mars:

- The energy distribution of the albedo particles to determine which of them enter behind Liulin-MO detectors shielding;
- The intensity of the albedo relative the GCR flux;
- Their angular distribution to calculate what part of the albedo flux hits Liulin-MO detectors.

In this work we use a modeling approach for estimation of the albedo contribution to the particle flux measured by Liulin-MO instrument in TGO Mars orbit. The modeling was performed with Atmospheric Radiation Interaction Simulator AtRIS (Banjac et al., 2018) implemented with the Mars atmospheric and regolith properties (Guo et al., 2019). The solar modulation condition for the input GCR is chosen as 400 MV from the Badhwar O'Neil 2014 model (O'Neil et al., 2015), which is a proxy of solar minimum. The modelled albedo spectra at 70 km height (Zhang et al., 2022) were used for the calculation of the albedo radiation fluxes at the TGO altitude.

A procedure for calculating the fluxes recorded by Liulin-MO detectors, including GCR and albedo fluxes on the basis of the detectors shielding model has been developed. The GCR particle flux was calculated using the Badhwar O'Neil 2014 model for December 1, 2018. In our estimations we took into account only the contributions from albedo protons and alpha particles as dominating charged particles and from neutrons and gamma rays. An analysis of the ExoMars TGO spatial orientation effect on Liulin-MO detectors count rate was carried out. The measured and computed fluxes in Liulin-MO detectors are compared.

The article is organized as following: Section 2 presents short description of Liulin-MO instrument; Section 3 introduces and describes the methodology for estimation the particle flux in Liulin-MO detectors in MSO, including modeling the albedo spectra and procedure for calculation the fluxes recorded by Liulin-MO; Section 4 shows and

discusses the results from the calculations; Section 5 present comparison between measured and calculated fluxes and Section 6 summarizes the main results, concludes our study and shows future work.

2. Liulin-MO description

A detailed description of Liulin-MO, the detectors shielding, the methodology of measurement and measured parameters is given in Mitrofanov et al. (2018), Semkova et al. (2018, 2021). Here we present only a short introduction to the instrument and its parameters, relative to this research. The Liulin-MO particle telescope contains two dosimetric telescopes- BA and DC arranged at two perpendicular directions. Fig. 1. is a sketch of the sensor unit. Each pair of the dosimetric telescopes consists of two 300 μm thick, 20 × 10 mm area rectangular Si PIN photodiodes.

To meet the requirement to measure the energy deposited spectra in a wide energy range one of detectors in every telescope and its corresponding electronics measures and provides the energy deposition spectrum in the range 0.08–18 MeV (detectors B and D), and the other in the range 0.4–190 MeV (detectors A and C), each range covered by 256 energy channels. The energy deposition spectra of B (D) in the range ~ 0.08–15.9 MeV and of A (C) in the range ~ 16–190 MeV are later summarized and used to obtain the energy deposition spectrum in a single detector B(A) and D(C) in the two perpendicular directions BA and DC.

The parameters, provided by Liulin-MO simultaneously for two perpendicular directions have the following ranges: absorbed dose rate from 10^{-7} Gy h^{-1} to 0.1 Gy h^{-1}; particle flux in the range 0 - 10^4 cm^{-2} s^{-1}; energy deposition spectrum in the range 0.08–190 MeV. All events with energy deposition > 190 MeV are registered in the last spectral channels of A and C detectors and are considered as events with 190 MeV energy deposition in the subsequent calculations. The dose rates and the fluxes are resolved every minute, while the energy deposition spectra are resolved every hour.

The values $\sum_j n_j$ proportional to the flux for each detector are calculated on board from the corresponding energy deposition spectrum measured for a minute and are provided in the Liulin-MO output data. Here n_j is the number of particles in the spectral channel j.

In this paper we use the data for the particle fluxes provided by single detectors B(A) and D(C) in the energy deposition range > 0.08 MeV. As mentioned above all events with energy deposition > 190 MeV are registered and are considered as events with 190 MeV energy deposition in the measured fluxes.

In Fig. 2 the FREND and Liulin-MO orientations with respect to the spacecraft axes are shown. The FREND neutron detectors are oriented along the -Y axis, the Liulin-MO detectors are oriented along the - X and Z axes of the satellite. In Mars science orbit when TGO is pointed to nadir (along –Y axis), the angles between the detector's axes and nadir direction are 90° (Fig. 3). This is the nominal orientation.

The data from calculations and measurements of Liulun-MO fluxes presented below must be understood in the context of the shielding from the free-space radiation environment provided by the mass of materials surrounding the instrument's detectors. A model of Liulin-MO shielding was created on basis of the Russian standard GOST 25,645.204–83 (GOST, 1983), using the documentation of the FREND instrument and data for TGO spacecraft obtained from http://spaceflight101.com/exomars/trace-gas-orbiter-instruments and http://sci-lib.com/article1181.html. Using this model the shielding distribution probability density was calculated (Semkova et al., 2018, 2021). It was estimated that there are no significant differences in the shielding caused by the dosimeter itself plus the rest of FREND modules to any of the four Liulin-MO detectors. Representative for the shielding of Liulin-MO detectors is the central point between the detectors located at equal distances from the detectors.

3. Method for estimation the particle flux in Liulin-MO detectors in MSO

The developed methodology for estimation the particle flux in Liulin-MO detectors in MSO includes modeling the albedo spectra and procedure for calculation the GCR and albedo fluxes recorded by Liulin-MO, which accounts for different orientations of TGO.

3.1. Modeling the albedo spectra

The Atmospheric Radiation Interaction Simulator (AtRIS) (Banjac

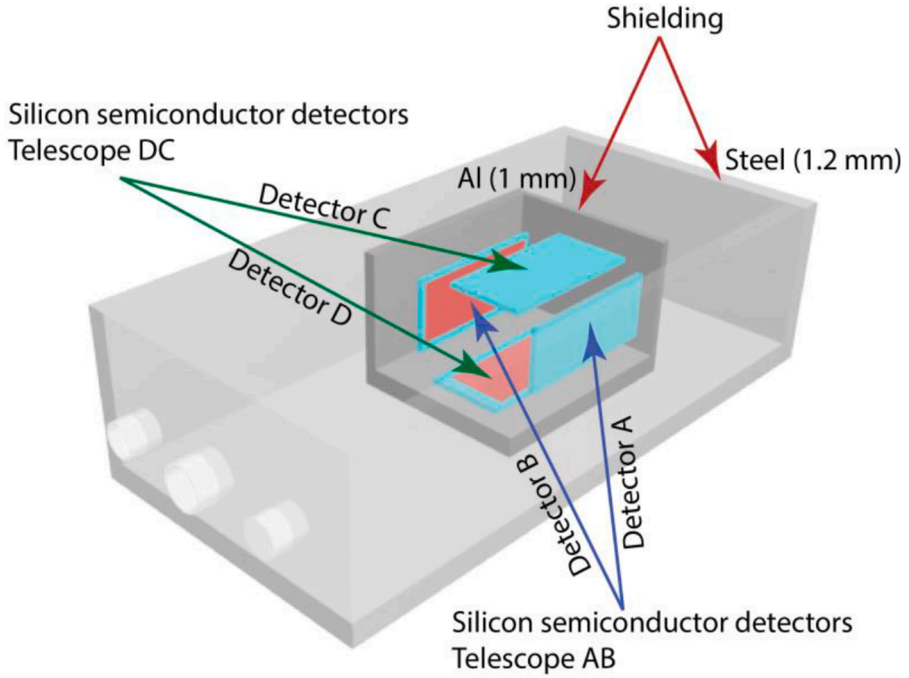

Fig. 1. A schematic view of Liulin-MO detectors' location in the dosimeter box (Semkova et al., 2021).

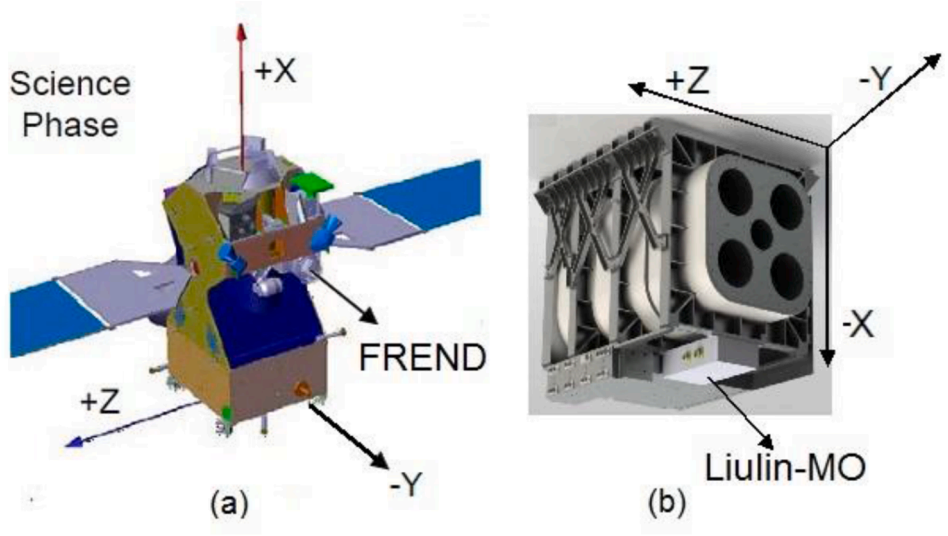

Fig. 2. (a) FREND location on TGO during the science phase; (b) FREND and Liulin-MO orientations with respect to the spacecraft axes (Semkova et al., 2021).

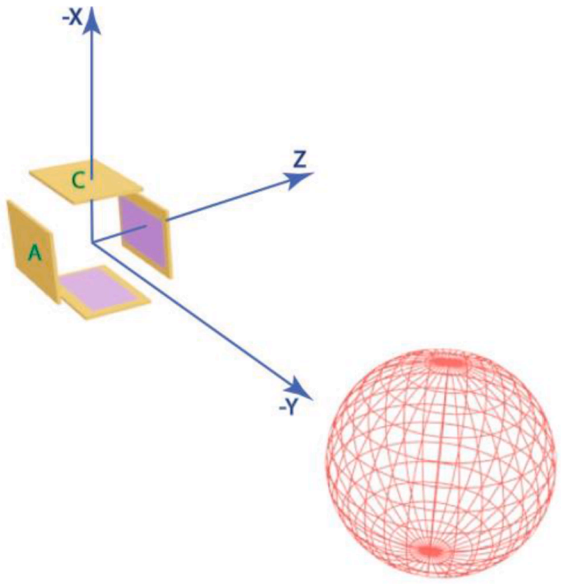

Fig. 3. Dosimeter axes orientation relatively to TGO nadir (Semkova et al., 2021).

et al., 2018; Guo et al., 2019) is based on Geant4, a Monte Carlo code used for simulating radiation transport covering interactions in a wide energy range (Agostinelli et al., 2003). AtRIS allows to set up specific planetary environments, considering specific composition and height of the atmosphere and different compositions of the regolith. The radiation propagates and generates secondaries which eventually reach the ground and, by interactions with the regolith, create upward secondaries.

In order to set up the Martian environment, we combine AtRIS with the Mars Climate Database (MCD, Forget et al., 1999, http://www-mars.lmd.jussieu.fr). MCD collects the meteorological fields as derived by simulations based on the General Circulation Model (GCM) of the Martian atmosphere and validated using available observational data. Vertical profiles of atmospheric properties including the composition (95% CO2) and density are loaded as the environment setup for AtRIS - see Guo et al. (2019) and Röstel et al. (2020) for more details on the combination of AtRIS and MCD. The surface radiation as observed by MSL/RAD shows also small changes due to the atmospheric diurnal and seasonal changes (Rafkin et al., 2014; Guo et al., 2021). Besides, Mars has many high mountains and low-altitude craters where the atmospheric thickness can be more than 10 times different from one another. Zhang et al. (2022) recently studied the influence of the atmospheric depths on the Martian radiation levels using AtRIS considering locations such as the top of Martian Olympus and the bottom of Hellas Planitia. This atmospheric effect is accounted for in the current study by using two extreme values of the surface pressure in the model: 82 Pa and 1200 Pa.

In a hydrostatic atmosphere, the atmospheric thickness directly corresponds to the surface pressure. In this work, we consider 80 atmospheric altitude layers up to 80 km above the Martian surface, evenly spaced in logarithmic scale. At the altitude of 70 km, the pressure is almost negligible as compared to the surface, which means that the atmosphere above 70 km plays a minimal role in the interaction with propagating cosmic rays and thus the upward radiation flux at this altitude can be used to extrapolate to the TGO orbit without taking into account the atmospheric interactions.

The regolithic composition is considered as a composition of 50% O, 40% Si, 10% Fe (mass fraction) and a density of 1.79 g/cm^2, which is close to that of SiO_2 (Zhang et al., 2022). Despite the regolithic composition can vary from place to place, here such composition is kept as fixed, as the interest of the work is focused on the radiation environment on orbit, and in particular on the albedo radiation, which would anyway average for different surface/subsurface scenarios. Also, recent works (Röstel et al., 2020; Da Pieve et al., 2021) have reported that the radiation environment (in terms of absorbed dose) on Mars changes only to small extent for different soil composition and that the subsurface radiation environment mostly depends on the regolithic column depth. However, the models actually suggested that the albedo neutrons, in particularly in the energy range below a few MeVs, can be influenced by the hydrogen and iron content in the Martian soil. The impact of the regolith composition on the albedo flux detected at the orbit can be a topic for future studies. A total depth of the regolith of 10 m is considered, as previous work has shown that this is a sufficient depth within which almost all particles fully stop (Röstel et al., 2020).

The detailed model setup for calculating the results used in this study can be found in Zhang et al. (2022). The energy-dependent GCR fluxes used as input in this work as calculated by the Badhwar O'Neil (BON) 2014 model are plotted in Fig. 4 for a solar modulation condition chosen as 400 MV which is a proxy of solar minimum period 2018–2019, of interest here.

The upward particle spectra at 80 km altitude under two surface

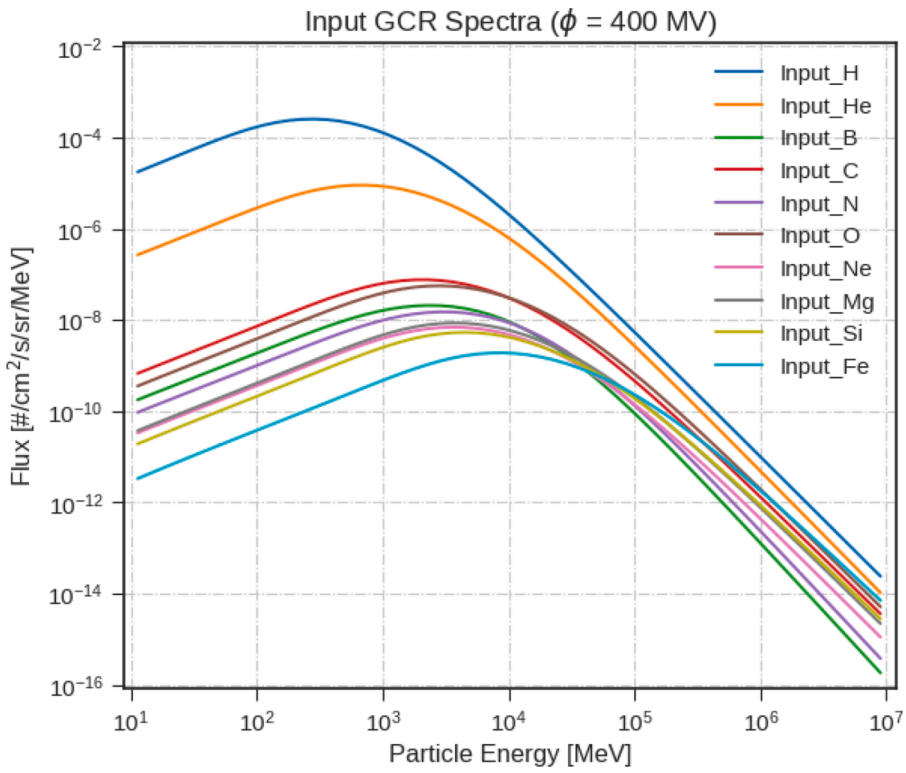

Fig 4. The deep-space GCR spectra used as input in this work as calculated by the BON 2014 model with the solar modulation parameter chosen as 400 MV.

pressures (82 Pa and 1200 Pa) are plotted in Fig. 5. The upward particles flux includes protons, neutrons, Helium ions and gammas. The spectra are energy-, angle- and time-differential (unit of *#/sec*/MeV/sr/cm2).

3.2. *Procedure for calculating the fluxes recorded by Liulin-MO detectors*

Calculations were carried out on the basis of the detectors shielding model described in Section 2. The calculations were performed in the coordinate system, the direction of the axes of which is shown in Fig. 2.

The center of the coordinate system used in the calculations is in the central point between the detectors, which is located at equal distances from the detectors. 64,802 rays coming out of this point were set. The direction of each ray was set in the form of guiding cosines; each ray was assigned a solid angle through the center of which this ray passed. The set of rays was chosen in such a way that all solid angles were equal to each other.

Then for each ray the shielding thickness along the path from the center of the coordinate system to the exit of the spacecraft was calculated. We will denote this thickness by the symbol *h*. The value *h*, calculated for each beam, will be used in further calculations.

Based on the results of the calculations, a file was created in which each ray corresponds to one line specifying the guiding cosines of the ray and the shielding thickness. Then this file was supplemented with data of GCR fluxes or albedo particles corresponding to each ray.

The coordinate system shown in Fig. 2 was also used to indicate the orientation - the position of Mars relative to the spacecraft. The direction to the center of Mars was set as angles θ and φ in a spherical coordinate system, where the angle θ was calculated from the direction of the Z axis, and the angle φ was calculated from the X axis towards the Y axis to project the direction to Mars onto the XY plane.

The values of $\theta = 90^\circ$ and $\varphi = -90^\circ$ correspond to the standard position of the spacecraft when FREND instrument "looks" at Mars, i.e. Mars is in the direction of the - Y axis. This is the nominal orientation of Liulin-MO detectors (see Fig. 3).

According to the values of the angles θ and φ and the altitude of TGO for each ray it is determined whether it is directed towards the surface of Mars or points into "free space". For the rays directed towards the surface of Mars and into the "free space", the average shielding thickness was calculated separately. It turned out the shielding to be smallest from the side facing Mars with the orientation set by the parameters $\theta = 120^\circ$ and $\varphi = -130^\circ$. In this case, the Liulin-MO detectors are shielded on the side facing Mars only by the structure of the dosimeter itself.

3.2.1. *GCR flux calculation*

The GCR particle flux was calculated using the OLTARIS tools (https://oltaris.larc.nasa.gov/). We used data from the Badhwar-O'Neill GCR model 2014 for December 1, 2018 and the calculation was made for a set of aluminum thickness from 0 to 400 g cm^{-2}. For each of the rays directed into the "free space" the flux of charged GCR particles behind the shielding thickness corresponding to this ray was calculated. Then the contribution to the detector's counting rate was calculated taking into account the orientation of the ray relative to the axis of the detector. Next, integration was performed within the solid angle corresponding to the "free-space" rays.

3.2.2. *Calculation of the proton and alpha albedo flux*

For each ray pointing towards Mars the shielding thickness and the incident to the detectors flux, accounting for Mars shading were calculated. The flux dependence on the shielding thickness is calculated using the method of linear interpolation from tables. A more detailed description of the procedure for calculating the proton albedo flux is given below.

First for each ray directed towards the surface of Mars, the distance to the point on the surface of the sphere representing Mars where this ray "ends" was calculated. Next, the angle between the local direction to the zenith at this point of the surface and the direction to the spacecraft was calculated, as well as the surface area, which is within the solid angle as was originally divided into 64,802 zones.

Then the flux of protons coming towards the detector from this area of the top of Martian atmosphere was calculated. To do this the albedo

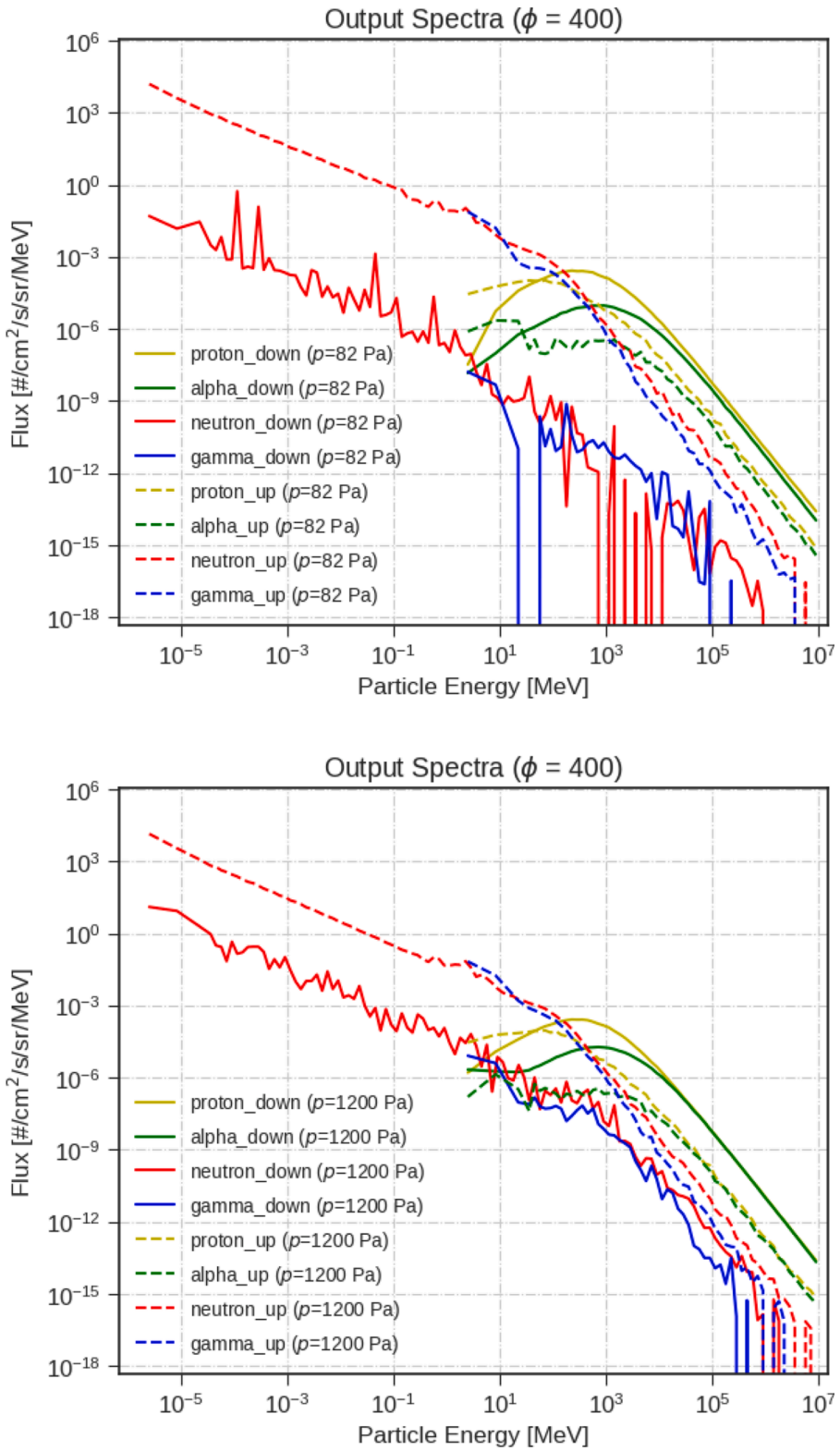

Fig. 5. The output spectra from the model at the top of the atmosphere with the surface pressure of 82 Pa (top) and 1200 (bottom) averaged within either upward or downward directions.

table was calculated from the upward proton differential spectrum for surface pressure 1200 Pa or 82 Pa (Fig. 5). From the differential spectrum *j(E)* in cm^{-2} s^{-1} MeV^{-1} sr^{-1}, the integral spectrum *J(>E)* in cm^{-2} s^{-1} sr^{-1} was calculated. Then, the tabular values of the proton energy in the integral spectrum were compared with the values of the proton ranges in aluminum. The resulting table was further used for interpolation the dependence of the flux on the shielding thickness.

When calculating the flux incident on the detector from different directions the following cosine angular distribution over the zenith angle *l* was considered:

$$(n+1)\cdot j(h)\cdot\cos^n(\lambda)$$

The *(n + 1)* coefficient used further reflects the case when the albedo flux in dependence of the shielding thickness *j(h)* is the mean for all upward directions. In case *j(h)* is the flux directed to zenith, the coefficient is 1 and all results for the albedo flux should be divided by *(n + 1)*.

A similar technique was used to calculate the contribution from helium nuclei. Only the range–energy dependence table for protons was replaced with the corresponding table for helium nuclei.

3.2.3. Calculation of the neutron and gamma albedo

While the detection efficiency of a silicon detector to high-energy protons and helium nuclei trapped in its sensitive area is close to 100%, the efficiency to neutrons and gamma radiation registration is much less. Therefore, the first step was to evaluate the corresponding values of the registration efficiency for neutrons and gamma radiation. The detector sensitivity to neutrons and gamma was taken from the data of on ground physical calibrations of Liulin-MO dosimeter. The calibration data obtained from Dubna Cf-252 neutron source and the data from Cs-137 gamma radiation source calibration performed at the VNIIFTRI metrological center near Moscow were used.

3.2.3.1. Assessment of sensitivity to gamma radiation. The energy of the gamma quanta of Cs-137 source used for the calibration is 0.662 MeV. For monoenergetic gamma quanta, the connection of kerma with the flux of gamma quanta is given by the relation (Ivanov, 1988):

$K = 1.6\ 10^{-10}\ \mu_a\ E\ \Phi$, where: K - kerma, Gy; μ_a is the energy conversion coefficient, $cm^2\ g^{-1}$; E is the energy of gamma quanta, MeV; Φ is the total flux of gamma quanta, cm^{-1}; For gamma quanta with energies less than 3 MeV, K practically coincides with the absorbed dose. Therefore Φ can be calculated from the dose value, and the flux F ($cm^{-2}\ s^{-1}$) can be calculated from the dose rate.

The corresponding value of the energy conversion coefficient in silicon μ_a is 0.0294 $cm^2\ g^{-1}$, and the kerma value for the flux of 1 quantum cm^{-2} is 3.11 10^{-12} Gy cm^2.

Table 1 shows the values obtained during calibration and the values of the incident gamma-ray flux, as well as the values of the count rates recorded during the measurement.

The dose rate values were determined on the basis of the distance to the reference radiation source, the number of particles during the observation intervals were measured by Liulin-MO. The remaining parameters are result of processing.

The decrease in the registration efficiency at the third, highest dose rate can be caused by missing registrations of particles due to overload of the electronics in this mode. Based on the results of processing, a value of the gamma-quantum registration efficiency equal to 0.0056±0.0017 was selected for further evaluations.

3.2.3.2. Neutron sensitivity assessment. The sensitivity of Liulin-MO to neutrons was taken from the data of its calibration performed using the Cf-252 source. The flux from this source on August 13, 2014, when the calibration was carried out was 2.99 $10^6\ s^{-1}$. The dependence of the number of records per second in the detectors on $1/R^2$ and the linear approximation of this dependence were obtained. For further estimates the slope coefficient of the approximating straight line is taken equal to 5200 ± 803 $cm^2\ s^{-1}$.

The counting rate obtained by this approximation for a distance of 100 cm is $N = (5200 \pm 803\ cm^2\ s^{-1})/100^2\ cm^2 = 0.52 \pm 0.08\ s^{-1}$.

The neutron flux which gives a source at this distance for activity on August 13, 2014 is determined by the formula $F = (2.99\ 10^6\ s^{-1})/(4\pi\ 100^2\ cm^2) = 23.78\ cm^{-2}\ s^{-1}$.

Dividing the above counting rate by the neutron flux that the source gives at distance of 100 cm we obtain a coefficient characterizing the sensitivity of the detector to neutrons: $K = (0.52 \pm 0.08\ s^{-1})/23.8\ cm^{-2}\ s^{-1} = (0.022 \pm 0.0034)\ cm^2$. Dividing K by the detector area of 2 cm^2 the sensitivity of the detector to neutrons is then 0.011 ± 0.0017.

The albedo neutron spectrum differs from the fission neutron spectrum of Cf-252 on which the calibrations were carried out. The spectrum of fission neutrons contains a higher proportion of fast neutrons. However, due to the lack of more suitable data, the value obtained above is taken. Perhaps in the future it will be useful to clarify the sensitivity to the albedo neutron spectrum by conducting computational modeling of the neutron registration process for both spectra. It should also be noted that in the assessed sensitivity, the possible contribution to the counting rate of the detectors of the accompanying gamma radiation Cf-252 was not taken into account, which could overestimate the coefficient obtained and, accordingly, all further estimates obtained. Therefore, at this stage of the analysis, further calculated values of the contribution of neutrons to the count rate of detectors should be considered as an upper estimate.

3.2.3.3. A method for calculating the contribution to the detectors counting rate of the albedo neutron and gamma-quantum flux. The calculation of the albedo neutron and gamma radiation flux was carried out in a way similar to that of albedo protons. The total number of gamma radiation was calculated by integrating the corresponding upward spectra. The spectra and the full flux of albedo neutrons contain a large share with energies too small to cause a hit above 80 keV deposited energy threshold in the detector (see Fig. 5). The calculations show that the minimum energy of a neutron capable of imparting an energy of 80 keV to a silicon nucleus is 601 keV. In reality, in order to obtain a noticeable cross section for the generation of recoil nuclei of above 80 keV threshold energy, an initial energy of 800–900 keV is required. That's why we have calculated the integral upward neutron spectra *J>(0.9 MeV)* in $cm^{-2}\ s^{-1}\ sr^{-1}$ and used them for the estimation of the albedo neutron flux in the detectors.

Since the calculation taking into account the neutron spectrum is very laborious both in terms of the passage of neutrons through the spacecraft materials and in terms of the interaction of the resulting spectrum with the detector material and the surrounding structural elements, a very approximate estimate was made for the characteristic

Table 1

Experimental and evaluation results from calibration with gamma. In the columns from left to right is shown: Experimental values: Dose rate values determined on the basis of the distance to the reference radiation source; Minimal and maximal number of registration in each of the detectors and mean value for two detectors number of registrations. As an uncertainty of the mean value is taken the maximum deviation of the measured value from the average over a series of measurements with detectors B and D; Evaluation results: The gamma quanta flux - calculation based on dose rate and the mean value of the registrations divided by the detectors area and time of measurement; Efficiency of gamma-quantum registration obtained by dividing the data in the previous 2 columns.

Experimental values						Evaluation results		
Dose rate μGy h^{-1}	Number of particles registered in 18 s					The gamma quanta flux $cm^{-2}\ s^{-1}$		
	Detector B		Detector D		Mean value	Calculation based on dose rate	Counting rate divided by the area and time	Efficiency of registration
	Min.	Max	Min.	Max				
2.74±0.14	39	57	39	62	49.25±12.8	244±12	1.37±0.36	0.0056±0.0017
25.76±1.28	428	502	472	539	485.25 ±57.2	2299±114	13.5 ± 1.6	0.0059±0.0010
1458±73	17,983	18,473	19,483	19,873	18,953 ±970	130,131±6515	526.5 ± 27	0.0041±0.0004

neutron energy. The value of 5 MeV was chosen as the characteristic neutron energy. For this energy the value of the range in aluminum at which the flux is attenuated by *e* times was estimated. According to https://portal.tpu.ru/SHARED/a/ALEXTPUFTF/uchebnye-mat/iinph/Tab1/radiation.pdf this value is close to 40 g cm^{-2}. When calculating the neutron flux that reached the detectors, an exponential attenuation law with an appropriate coefficient was applied.

For gamma radiation, the calculation method was similar, even the exponential attenuation coefficient was chosen the same.

For both neutron and gamma radiation through thin detector like the Liulin-MO detectors, the counting rate does not depend on the orientation of the detector. Therefore, the orientation of the rays relative to the detector was not taken into account, and the contribution to the counting rate was calculated by multiplying the flux that passed through the corresponding shielding thickness by the detector sensitivity coefficient defined above.

4. Results from the calculations of fluxes in Liulin-MO detectors and discussion

Based on the above-described method and procedure, calculations of the contribution to the counting rate of different components of the incident radiation were carried out.

Several calculations of the contributions of GCR and the proton albedo to the flux values that should be recorded by the detectors have been performed. Three variants of the spacecraft orientation and four variants of the angular distribution of albedo particles are considered. Table 2 shows the effect of orientation when the angular distribution of the albedo protons is $j(h)\cdot\cos(\lambda)$. When calculating the contribution of the albedo protons, in addition to the fluxes in the detectors, the values that would register an isotropic spherical detector of a unit area, placed in the same shielding conditions were calculated. This parameter is denoted as $J_{isotrop}$.

It can be seen that the effect of orientation, causing different shading of the GCR flux by Mars, significantly exceeds the effect from the albedo flux, the latter varies from 2.3% to 6.6% of the flux due to GCR themselves.

Table 3 shows the results of examining the effect of the angular distribution of albedo protons on the flux recorded by the detectors for detectors' orientation $\theta = 0$, $\varphi = 90$.

For B(A) detectors, whose axis is directed to the nadir, an effect of the exponent *n* on the recorded flux is practically absent. For the second pair of detectors the relative change is much larger but the absolute value of the differences is at the level of 0.01 particles per second, which is not discernible in the experimental data. This allows us to assume that the form of the angular distribution of albedo protons is not significant.

A series of calculations was carried out to assess the effect of orientation on the average thickness of the shielding in each direction. The calculations were carried out for the conditions of surface pressure 82 Pa (pres82 spectrum) and 1200 Pa (pres1200 spectrum), the exponent in the angular distribution $n = 1$. Along with the calculations for the albedo protons flux, the calculations for the alpha particles albedo flux were carried out using the same procedure. The results are shown in Table 4.

It can be seen that for a detector whose axis is oriented to the nadir, the contribution of the albedo protons to the recorded flux can reach 0.12–0.15 cm^{-2} s^{-1}. At a horizontal orientation of the axis, this contribution is reduced by almost twice. The contribution of the albedo alpha particles turned out to be about 20 times less.

The results for the neutron and gamma albedo contribution to the

Table 3
Estimation of the effect of the albedo protons angular distribution on the flux recorded by the detectors. In the columns from left to right is shown: Exponent in the formula $cos^n\lambda$ of the angular distribution over the zenith angle l; Calculated GCR flux in the detectors; Calculated albedo protons flux for surface pressure 1200 Pa.

Exponent *n* in distribution $cos^n\lambda$	GCR contribution to the registered flux cm^{-2} s^{-1}		Albedo protons contribution to the registered flux cm^{-2} s^{-1} for surface pressure 1200 Pa		
	B(A)	D(C)	J isotrop	J B(A)	J D(C)
0 (isotropic distribution)	1.63	2.09	0.175	0.108	0.080
1	1.63	2.09	0.149	0.108	0.058
2	1.63	2.09	0.137	0.108	0.047
3	1.63	2.09	0.13	0.108	0.04

Table 4
Calculation of proton and alpha particles albedo contribution to the registered flux. In the columns from left to right is shown:Upward spectra of protons and alpha particles under 82 Pa and 1200 Pa pressure; Spacecraft (detectors) orientation angles θ and φ; Average shielding thickness of the detectors on the side facing Mars; Estimated flux in the detectors of the corresponding particle in 1st column.

Spectrum under consideration	S/c orientation angles		Average shielding thickness on the side facing Mars, g cm^{-2}	Estimated contribution to the registered flux, cm^{-2} s^{-1}	
	θ	φ		Detector B(A)	Detector D(C)
pres82_Output_proton	90	90	28.9	0.0716	0.0648
	90	180	9.7	0.0867	0.1527
	120	-130	3.2	0.1082	0.1113
pres1200_Output_proton	90	90	28.9	0.0575	0.0514
	90	180	9.7	0.0709	0.1247
	120	-130	3.2	0.0890	0.0915
pres82_Output_alpha	90	90	28.9	0.0031	0.0029
	90	180	9.7	0.0033	0.0059
	120	-130	3.2	0.0039	0.0040
pres1200_Output_alpha	90	90	28.9	0.0030	0.0028
	90	180	9.7	0.0031	0.0056
	120	-130	3.2	0.0037	0.0038

Table 2
Assessment of the effect of detectors' orientation on the flux recorded by them. In the columns from left to right is shown: altitude of TGO; Spacecraft (detectors) orientation angles θ and φ; Description of the detectors axes orientation; Calculated GCR flux in the detectors; Calculated albedo protons flux in an isotropic spherical detector of a unit area and in the detectors for surface pressure 1200 Pa.

Altitude km	Orientation angles, degree		Orientation description	GCR contribution to the registered flux cm^{-2} s^{-1}		Albedo protons contribution to the registered flux cm^{-2} s^{-1} for surface pressure 1200 Pa		
	θ	φ		B (A)	D (C)	J $_{isotrop}$	J B(A)	J D(C)
400	0	90	The axis of the detector B(A) is directed to the nadir, and the axis of detector D(C) is directed to the horizon	1.63	2.09	0.149	0.108	0.058
400	90	0	The axis of the detector B(A) is directed to the horizon, and the axis of the detector D(C) is directed to the nadir	2.11	1.64	0.111	0.049	0.078
400	90	90	The axes of both detectors are directed to horizon	2.1	2.1	0.134	0.058	0.051

registered flux in dependence on the spacecraft orientation (and on the average shielding thickness on the side facing Mars) are shown in Table 5. In addition to the three orientation options discussed earlier, another line was added, in which the exponential attenuation of the flux with thickness was not taken into account in the calculation.

The results from the calculations of the albedo when Liulin-MO sensors look at 90° to nadir show that the contribution of the total albedo (protons, alpha, neutrons and gamma) to the measured total flux from GCR and albedo is 4.1% for detectors B(A) and D(C) for surface pressure conditions 1200 Pa. The corresponding values for surface pressure conditions 82 Pa are 5% for detectors B(A) and D(C). These values are lower than the estimated albedo contribution to the measured flux from the statistical studies.

5. Comparison of the calculated and measured by Liulin-MO fluxes in TGO Mars orbit

Calculations of the total flux in Liulin-MO detectors for detectors axes orientation to the horizon and to nadir were made for 1 December 2018. The calculations were conducted for the two extreme surface pressure conditions 82 and 1200 Pa.

On 1 December 2018 TGO was oriented nominally (-Y axis oriented to Mars). In the experimental data from December 2018 several cases are observed when TGO changes its orientation relative to the direction to Mars by about 90°, the closest cases to the moment of calculations are on 6 and 9 December 2018. In Fig. 6 are plotted the time profiles of the fluxes registered by detectors B(A) and D(C), angles between the axes of the detectors and the direction to the center of Mars and altitude of TGO for 9 December 2018 from 15:00 to 21:00 UT. Most of the time –Y axis of TGO is oriented along nadir and the angle between detector's axis and Mars direction is ~ 90° as seen from Figs. 2b and 3. The dominant part of data presented in Fig. 6 relate to this orientation. The sharp drops of the measured flux appear when the angle between detector's axis and Mars direction approaches zero or 180°. Similar changes in the TGO orientation and corresponding drops of the measured flux are observed on 6 December 2018 from 15:00 to 21:00 UT. We choose the measurements conducted on 6 and 9 December 2018 from 15:00 to 21:00 UT for comparison with the calculations.

Table 5
Calculation of the neutron and gamma albedo contribution to the registered flux. In the columns from left to right is shown: Upward spectra of neutrons and gamma under 82 Pa and 1200 Pa pressure; Integral flux of albedo neutrons and integral gamma albedo flux calculated from the corresponding upward spectrum in the 1st column. Spacecraft (detectors) orientation angles θ and φ; Average shielding thickness of the detectors on the side facing Mars; Estimated flux of neutrons or gamma in the detectors.

Spectrum under consideration	Flux cm^{-2} $sr^{-1}s^{-1}$	S/c orientation angles degree θ	φ	Average shielding thickness on the side facing Mars g cm^{-2}	Estimated contribution to the registered flux cm^{-2} s^{-1}
Upward neutrons	0,48	90	90	28.9	0,020
with E>0,9		90	180	9.7	0,030
MeV for		120	-130	3. 2	0,034
pressure 82 Pa.				0	0,037
Upward neutrons	0,34	90	90	28.9	0,015
with E>0,9		90	180	9.7	0,021
MeV for		120	-130	3.2	0,024
pressure 1200 Pa.				0	0,026
Upward gamma	0.42	90	90	28.9	0.009
rays for		90	180	9.7	0.013
pressure 82 Pa.		120	-130	3.2	0.015
				0	0.016
Upward gamma	0.45	90	90	28.9	0.010
rays for		90	180	9.7	0.014
pressure 1200		120	-130	3.2	0.016
Pa				0	0.017

In Table 6 we compare the calculated fluxes for 1 December 2018 for different orientations and surface pressure conditions and the measured fluxes on 6 and 9 December 2018 from 15:00 to 21:00 UT. From the measurements the average and the minimum values of the fluxes over the period of measurement were determined. In Table 6 for the detectors axes orientation to the horizon the average values of the corresponding measured fluxes are shown, the minimum values of the measured flux are attributed to the orientation of the detectors axes in nadir.

The results show that the measured fluxes exceed the calculated values for both surface pressure conditions 82 Pa and 1200 Pa and for all orientations. The minimum difference between the measured and calculated fluxes is 20% (within the uncertainty of the measurement). It relates to orientation of detector B(A) axis along nadir and surface pressure 82 Pa.

For pressure conditions 1200 Pa with the usual TGO orientation, when the axes of both detectors are directed horizontally, the measured fluxes exceed the calculated values at least by 27.4% for detector B(A), and by 30.1% for detector D(C).

For the pressure conditions 82 Pa when the axes of both detectors are directed horizontally, the measured fluxes exceed the calculated values by at least 27.4% for detector B(A), and by at least 29% for detector D (C).

The orientation change effect is comparable for the calculated and measured fluxes. The measured flux in nadir orientation is 78% - 80% of that measured in horizontal orientation. The calculated flux in nadir orientation is 80% - 81% of the calculated one in horizontal orientation for pressure condition 1200 Pa; for pressure condition 82 Pa the calculated flux in nadir orientation is 81% of the calculated one in horizontal orientation.

There are several facts that are different between the simulation setup and the measurement setup that could potentially add to the discrepancy between the measured and calculated fluxes: (1) Additional Anomoulous Cosmic Rays (ACR) are not included in the BON GCR model, but they may also contribute to the measured charged particle flux. ACRs originate from interstellar neutral gas that flows into the heliosphere and is ionized by solar radiation or solar wind and then are accelerated at the termination shock of solar wind. ACRs dominate at low energies of the GCR spectra (generally below ~ 100 MeV/nuc) and could make an extra contribution to the observed flux. (2) The use of 1 AU GCR spectrum in calculation of the GCR and albedo contribution to the measured flux in TGO MSO can lead to decrease in the calculated flux by about 2% (Geiseler et al. 2008); (3) In addition to the albedo particles from Mars, secondary charged particles, neutrons, and gamma-rays are generated in the spacecraft body by GCRs, and they could be measured by Liulin-MO detector. When calculating the GCR contribution to the detector count rate, the contribution of primary and secondary protons and heavier nuclei was taken into account. The contribution of secondary leptons, neutrons, and gamma radiation was not taken into account. After the upgrade of the OLTARIS site in March 2022, it became possible to estimate the lepton fluxes, among which only electron fluxes show noticeable values. The possible contribution of secondary electrons and neutrons to the recorded count rate was calculated. The same detector protection model as described in Section 2 and the calculation method described in Section 3.2.1 were used. The calculations show that the contribution of electrons to the detectors count rate can reach almost 10%. The calculation of the dependence of the number of secondary neutrons on the thickness of the shield, obtained from the OLTARIS site for the BON 2014 model, gave a value of 5.06 neutrons cm^{-2} s^{-1} in free space and 3.64 neutrons cm^{-2} s^{-1} in TGO orbit. Taking into account the sensitivity coefficient obtained for neutrons, this gives an estimate of the detectors count rate from secondary neutrons of 0.08 s^{-1}. Accounting for secondary radiation can increase the calculated flux estimates by 8–12%, which reduces the gap with the measurement results; (4) Albedo particles like other hydrogen isotopes and lower-abundant heavier ions that would have an influence in the count rate are not taken into account. In particular, the other hydrogen

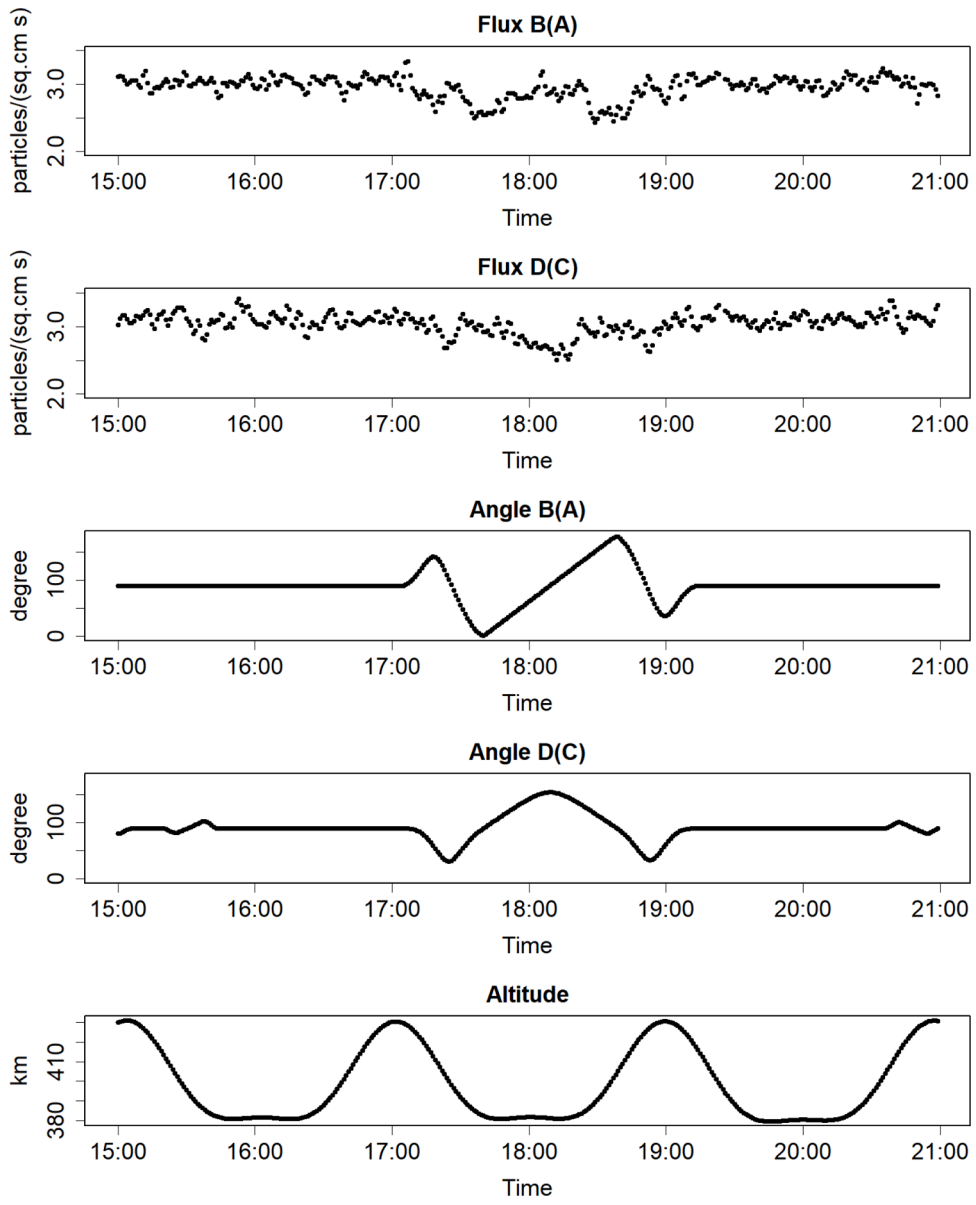

Fig. 6. From top to bottom - time profiles of the: flux registered by detector B(A); flux registered by detector D(C); angle between the axis of the detector B(A) and the direction to the center of Mars; angle between the axis of the detector D(C) and the direction to the center of Mars; altitude of TGO. Data are plotted for 9 December 2018 from 15:00 to 21:00 UT.

Table 6
Comparison between the calculated fluxes for 1 December 2018 for different orientations and two surface pressure conditions and the measured fluxes on 6 and 9 December 2018 from 15:00 to 21:00 UT. In the columns from left to right are shown: Spacecraft (detectors) orientation angles θ and φ; Total calculated flux in the detectors from GCR and albedo for pressure 82 Pa; Total calculated flux from GCR and albedo for pressure 1200 Pa; Measured flux on 06 December 2018; Measured flux on 09 December 2018.

Orientation angles, degree		Total calculated flux (GCR and albedo) $cm^{-2}\,s^{-1}$ Pressure 82 Pa		Total calculated flux (GCR and albedo) $cm^{-2}\,s^{-1}$ Pressure1200 Pa		Measured flux $cm^{-2}\,s^{-1}$, 06 December 2018		Measured flux $cm^{-2}\,s^{-1}$, 09 December 2018	
θ	φ	Detector B(A)	Detector D(C)	Detector B(A)	Detector D(C)	Detector B(A)	Detector D(C)	Detector B(A)	Detector D(C)
0	90	1.81	2.21	1.78	2.19	2.33±0.12	No data	2.28±0.11	No data
90	0	2.2	1.77	2.19	1.74	No data	2.49±0.13	No data	2.42±0.12
90	90	2.22	2.21	2.2	2.19	2.98±0.15	3.00±0.15	2.98±0.15	3.08±0.15

isotopes could have an equal or higher influence on the count rate than alphas. The potential influence of all these particles on the total albedo flux might be small, but they can be a topic for future studies.

6. Conclusions

- A method for estimation the particle flux in Liulin-MO detectors in TGO circular Mars science orbit and a procedure for its calculation have been developed. The calculations were carried out on the basis

of a detectors shielding model. GCR and Mars albedo radiation contribution to the detectors count rate was taken into account. The GCR particle flux was calculated using the BON 2014 model for December 1, 2018 and using OLTARIS. The modelled albedo spectra of protons, helium ions, neutrons and gamma rays at 70 km height obtained from AtRIS were used for the calculation of the albedo radiation fluxes at the TGO altitude. The energy-dependent GCR fluxes as calculated by the BON 2014 model are used as input in the modeling of the albedo. The sensitivity of the Liulin-MO semiconductor detectors to neutron and gamma radiation has been assessed in order to calculate the contribution of the neutrals to the registered flux. In the calculation of the albedo neutron flux only neutrons with energy larger than 0.9 MeV necessary to obtain a noticeable cross section for the generation of recoil nuclei of above-threshold energy in the silicon detector are taken into account.

- The result of this work provides useful insights on the radiation environment at the altitude of TGO orbit around Mars. The obtained results suggest that the contribution of albedo radiation can be about 4–5% of the total flux from GCR and albedo at the TGO altitude. However, the results show that the effect of TGO orientation, causing different shading of the GCR flux by Mars, significantly exceeds the effect from the albedo contribution to the flux in Liulin-MO detectors. The measured fluxes exceed the calculated values of GCR plus albedo flux for both extreme surface pressure conditions 82 Pa and 1200 Pa and for all orientations by at least 20%. This minimum difference between the measured and calculated flux relates to orientation of detector axis along the nadir and surface pressure 82 Pa. When the axes of the detectors are directed horizontally, the measured fluxes exceed the calculated values by at least 27.4%. There are several facts that are different between the simulation setup and the measurement setup that could potentially add to this discrepancy as discussed in Section 5. Accounting for the ACR contribution, secondary radiation and the gradient of GCR spectrum from 1 AU to 1.5 AU, the calculated flux may increase to match the measurement results. The result can serve for the benchmarking of GCRs models at Martian orbit.
- Future studies are planned including: a) Improving the quality of computational estimates, by conducting a three-dimensional modeling of the passage of cosmic radiation through the TGO, FREND and Liulin-MO structural elements; b) Calculation of dose rate in Liulin-MO detectors and comparison with the measured values in ExoMars TGO MSO; c) Calculation of the particle fluxes and dose rate in the free space, based on Liulin-MO measurements in ExoMars TGO MSO which can serve for benchmarking of the GCR models for free space radiation. The results could be used for further assessing the absorbed dose, LET spectra, and effective dose inside a human body for future crewed mission in orbit around Mars.

Declaration of Competing Interest

The authors declare that they have no known competing financial interests or personal relationships that could have appeared to influence the work reported in this paper.

Acknowledgements

The Mars modeling work is support by the Strategic Priority Program of the Chinese Academy of Sciences (Grant No. XDB41000000), the National Natural Science Foundation of China (Grant No. 42074222) and the CNSA pre-research Project on Civil Aerospace Technologies (Grant No. D020104). The work in Bulgaria is supported by grant KP-06 - Russia 24 from the Bulgarian National Science Fund and by Contract No 4000133961/21/NL/SC funded by the Government of Bulgaria through an ESA Contract under the Plan for European Cooperating States. F. Da Pieve was supported from the Research Executive Agency (until March 2021) and from the Health and Digital Executive Agency (from April 2021) under the EU's Horizon 2020 Research and Innovation program (grant ID 776410). The work of the Institute of Biomedical Problems of the Russian Academy of Sciences specialists was partially supported from project 65.2 of the Russian Academy of Sciences. At the Space Research Institute, Russian Academy of Sciences the presented work is supported by Grant 19–52–18009 of the Russian Foundation for Basic Research. The measured data by Liulin-MO used in this paper are available at http://esa-pro.space.bas.bg/LIULIN_MO_MARS_2/. The ExoMars2016 SPICE Kernels used in the work are downloaded from https://www.cosmos.esa.int/web/spice/spice-for-exomars-2016. The authors are thankful to NASA Langley Research Center for the provided possibility to use for calculations OLTARIS: On-Line Tool for the Assessment of Radiation in Space. The authors are thankful to the reviewers for their valuable comments and suggestions that help to improve the quality of this work.

References

Agostinelli, S., Allison, J., Amako, K., Apostolakis, J., Araujo, H., Arce, P., et al., 2003. GEANT4: a simulation toolkit. Nuclear Instruments and Methods in Physics Research Section A 506 (3), 250–303.

Banjac, S., Herbst, K., Heber, B., 2018. The atmospheric radiation interaction simulator (AtRIS) - description and validation. J. Geophys. Res. Space Phys. 123. https://doi.org/10.1029/2018JA026042 (ja).

Benghin, V., Shurshakov, V., Semkova, J., Dachev, T., Maltchev, St., Tomov, B., Matviichuk, Yu., Dimitrov, P., Koleva, R., Krastev, K., Mitrofanov, I., Zelenyi, L., Malakhov, A., Mokrousov, M., Sanin, A., Litvak, M., Kozyrev, A., Tretyakov, V., Golovin, D., Nikiforov, S., Drobyshev, S.G., 2019. Comparison of Liulin-MO dosimeter radiation measurements during ExoMars 2016 TGO Mars circular orbit with dose estimations based on galactic cosmic ray models. In: 24-th annual WRMISS. Athens, Greece. September 3 - 5. https://wrmiss.org/workshops/twentyfourth/Benghin.pdf.

Da Pieve, F., Gronoff, G., Guo, J., Mertens, C., Neary, L., Gu, B., Koval, N., Kohanoff, J., Vandaele, A.C., Cleri, F., 2021. Radiation environment and doses on Mars at Oxia Planum and Mawrth Vallis: support for exploration at sites with high biosignature preservation potential. J. Geophys. Res. Planets 126 (1) e2020JE006488.

De Angelis, G., Wilson, J., Clowdsley, M., Qualls, G., Singleterry, R., 2006. Modeling of the Martian environment for radiation analysis. Radiat. Meas. 41 (9), 1097–1102.

Ehresmann, B., Burmeister, S., Wimmer-Schweingruber, R.F., Reitz, G., 2011. Influence of higher atmospheric pressure on the Martian radiation environment: implications for possible habitability in the Noachian epoch. J. Geophys. Res. Space Phys. 116 (A10) https://doi.org/10.1029/2011ja016616.

Forget, F., Hourdin, F., Fournier, R., Hourdin, C., Talagrand, O., Collins, M., Lewis, S.R., Read, P.L., Huot, J.-P., 1999. Improved general circulation models of the Martian atmosphere from the surface to above 80 km. J. Geophys. Res. 104, 24155. https://doi.org/10.1029/1999JE001025.

Gieseler, J., Heber, B., Dunzlaff, P., et al., 2008. The radial gradient of galactic cosmic rays: 657 Ulysses KET and ACE CRIS Measurements. Int. Cosmic Ray Conf. 1 (658), 571–574.

Patrícia, Gonçalves, Luísa, Arruda, Marco, Pinto, 2022. Validation of dMEREM, the detailed mars energetic radiation environment model, with RAD data from the surface of Mars. Front. Astron. Space Sci. 9 https://doi.org/10.3389/fspas.2022.833144.

GOST, 1983. The Method of Calculating the Shielding of Points Inside the Phantom, 25645.204-83. Gosstandart, Moscow.

Gronoff, G., Norman, R.B., Mertens, C., 2015. Computation of cosmic ray ionization and dose at Mars. I: a comparison of HZETRN and Planetocosmics for proton and a particles. Adv. Space Res. 55 (7), 1799–1805.

Guo, J., Zeitlin, C., Wimmer-Schweingruber, R.F., Rafkin, S., Hassler, D.M., Posner, A., et al., 2015. Modeling the variations of Dose Rate measured by RAD during the first MSL Martian year: 2012–2014. Astrophys. J. 810 (1), 24.

Guo, J., Zeitlin, C., Wimmer-Schweingruber, R., Hassler, D.M., Köhler, J., Ehresmann, B., Böttcher, S., Böhm, E., Brinza, D.E., 2017. Measurements of the neutral particle spectra on Mars by MSL/RAD from 2015 to 11-15 to 2016-01-15. Life Sci. Space Res. (Amst) 14, 12–17.

Guo, J., Banjac, S., Rostel, L., et al., 2019. Implementation and validation of the GEANT4/AtRIS code to model the radiation environment at Mars. SWSC 9, A2.

Guo, J., Zeitlin, C., Wimmer-Schweingruber, R.F., Hassler, D.M., Ehresmann, B., Rafkin, S., Wang, Y., 2021. Radiation environment for future human exploration on the surface of Mars: the current understanding based on MSL/RAD dose measurements. Astron. Astrophys. Rev. 29 (1), 1–81. https://doi.org/10.1007/s00159-021-00136-5.

Ivanov, V.I., 1988. Dosimetry course: a Textbook For Universities, 4th ed. Energoatomizdat, Moscow (in Russian).

Kim, M.-H.Y., Cucinotta, F.A., Nounu, H.N., Zeitlin, C., Hassler, D.M., Rafkin, S.C.R., 2014. Comparison of Martian surface ionizing radiation measurements from MSL-RAD with badhwar-O'Neill 2011/HZETRN model calculations. J. Geophys. Rese. Planets 119 (6), 1311–1321. https://doi.org/10.1002/2013JE004549.

Knutsen, E.W., Witasse, O., Sanchez-Cano, B., Lester, M., Wimmer-Schweingruber, R.F., Denis, M., Godfrey, J., Johnstone, A., 2021. Galactic cosmic ray modulation at Mars and beyond measured with EDACs on Mars Express and Rosetta. A&A 650, A165.

Krastev, K., Semkova, J., Koleva, R., Bankov, N., Benghin, V., Drobishev, S., 2019. The shading effect for doses and galactic cosmic rays fluxes measured by Liulin. Eleventh workshop "solar influences on the magnetosphere, ionosphere and atmosphere". In: Book of Proceedings, pp. 31–34. https://doi.org/10.31401/WS.2019.proc. ISSN: 2367-7570.

Matthiä, D., Berger, T., Mrigakshi, A.I., Reitz, G., 2013. A ready-to-use galactic cosmic ray model. Adv. Space Res. 51, 329–338. https://doi.org/10.1016/j.asr.2012.09.022.

Matthiä, D., Ehresmann, B., Lohf, H., Kohler, J., Zeitlin, C., Appel, J., et al., 2016. The Martian surface radiation environment - a comparison of models and MSL/RAD measurements. J. Space Weather Space Climate 6, A13.

Matthiä, D., Hassler, D.M., deWet, W., Ehresmann, B., Firan, A., et al., 2017. The radiation environment on the surface of Mars - Summary of model calculations and comparison to RAD data. Life Sci. Space Res. (Amst) 14, 18–28.

Matthiä, D., Berger, T., 2017. The radiation environment on the surface of Mars - Numerical calculations of the galactic component with GEANT4/PLANETOCOSMICS. Life Sci. Space Res. 14, 57–63.

McKenna-Lawlor, S., Gonçalves, P., Keating, A., Morgado, B., Heynderickx, D., Nieminen, P., et al., 2012. Characterization of the particle radiation environment at three potential landing sites on Mars using ESAs MEREM models. Icarus 218 (1), 723–734.

Mitrofanov, I., Malakhov, A., Bakhtin, B., Golovin, D., Kozyrev, A., Litvak, M., Mokrousov, M., Sanin, A., Tretyakov, V., Vostrukhin, A., Anikin, A., Zelenyi, L.M., Semkova, J., Malchev, S., Tomov, B., Matviichuk, Y., Dimitrov, P., Koleva, R., Dachev, T., Krastev, K., Shvetsov, V., Timoshenko, G., Bobrovnitsky, Y., Tomilina, T., Benghin, V., Shurshakov, V., 2018. Fine Resolution Epithermal Neutron Detector (FREND) onboard the ExoMars Trace Gas Orbiter. Space Sci. Rev. 214, 86. https://doi.org/10.1007/s11214-018-0522-5. August 2018.

O'Neill, P., Golge, S., Slaba, T., 2015. Badhwar–O'Neill 2014 Galactic Cosmic Ray Flux Model. NASA/TP, 218569. Retrieved from. https://ntrs.nasa.gov/archive/nasa/casi.ntrs.nasa.gov/20150003026.pdf.

Rafkin, S.C., Zeitlin, C., Ehresmann, B., Hassler, D., Guo, J., et al., 2014. Diurnal variations of energetic particle radiation at the surface of Mars as observed by the Mars Science Laboratory Radiation Assessment Detector. J. Geophys. Res. (Planets) 119, 1345–1358.

Röstel, L., Guo, J., Banjac, S., Wimmer-Schweingruber, R.F., Heber, B., 2020. Subsurface radiation environment of Mars and its implication for shielding protection of future habitats. J. Geophys. Res. Planets 125 (3). https://doi.org/10.1029/2019JE006246 e2019JE006246.

Saganti, P.B., Cucinotta, F.A., Wilson, J.W., Simonsen, L.C., Zeitlin, C., 2004. Radiation climate map for analyzing risks to astronauts on the Mars surface from galactic cosmic rays. Space Sci. Rev. 110 (1–2), 143–156.

Schwadron, N.A., Boyd, A.J., Kozarev, K., Golightly, M., Spence, H., Townsend, L.W., Owens, M., 2010. Galactic cosmic ray radiation hazard in the unusual extended solar minimum between solar cycles 23 and 24. Space Weather 8. https://doi.org/10.1029/2010SW00056. S00E04.

Semkova, J., Koleva, R., Benghin, V., Dachev, T., Matviichuk, Yu., Tomov, B., Krastev, K., Maltchev, St., Dimitrov, P., Mitrofanov, I., Maklahov, A., Golovin, D., Mokrousov, M., Sanin, A., Litvak, M., Kozyrev, A., Tretyakov, V., Nikiforov, S., Vostrukhin, A., Fedosov, F., Grebennikova, N., Zelenyi, L., Shurshakov, V., Drobyshev, S., 2018. Charged particles radiation measurements with Liulin-MO dosimeter of FREND instrument aboard ExoMars Trace Gas Orbiter during the transit and in high elliptic Mars orbit. Icarus 303, 53–66. https://doi.org/10.1016/j.icarus.2017.12.034.

Semkova, J., Koleva, R., Benghin, V., Dachev, Ts., Matviichuk, Yu., Tomov, B., Krastev, K., Maltchev, S., Dimitrov, P., Bankov, N., Mitrofanov, I., Malakhov, A., Golovin, D., Mokrousov, M., Sanin, A., Litvak, M., Kozyrev, A., Nikiforov, S., Lisov, D., Anikin, A., Shurshakov, V., Drobyshev, S., 2020. Radiation environment in the interplanetary space and Mars orbit in 2016-2020 according measurements aboard ExoMars TGO. In: Proceedings of the Sixteenth International Scientific Conference Space, Ecology, Safety (SES 2020, pp. 23–34. http://space.bas.bg/SES/archive.html. e-ISSN 2603 –3321.

Semkova, J., Koleva, R., Benghin, V., Dachev, Ts., Matviichuk, Yu., Tomov, B., Krastev, K., Maltchev, S., Dimitrov, P., Bankov, N., Mitrofanov, I., Malakhov, A., Golovin, D., Mokrousov, M., Sanin, A., Litvak, M., Kozyrev, A., Nikiforov, S., Lisov, D., Anikin, A., Shurshakov, V., Drobyshev, S., 2021. Results from radiation environment measurements aboard ExoMars Trace Gas Orbiter in Mars science orbit in May 2018 - December 2019. Icarus, 114264. https://doi.org/10.1016/j.icarus.2020.114264. June.

Zeitlin, C., Boynton, W., Mitrofanov, I., Hassler, D., Atwell, W., Cleghorn, T.F., Cucinotta, F.A., Dayeh, M., Desai, M., Guetersloh, S.B., Kozarev, K., Lee, K.T., Pinsky, L., Saganti, P., Schwadron, N.A., Turner, R., 2010. Mars Odyssey measurements of galactic cosmic rays and solar particles in Mars orbit, 2002–2008. Space Weather 8. https://doi.org/10.1029/2009SW000563. S00E06.

Zhang, J., Guo, J., Dobynde, M.I., Wang, Y., Wimmer-Schweingruber, R.F., 2022. From the top of Martian Olympus to deep craters and beneath: mars radiation environment under different atmospheric and regolith depths. J. Geophys. Res. Planets 127. https://doi.org/10.1029/2021JE007157 e2021JE007157.